ATOMIC RESOLUTION STRUCTURES AND THE MECHANISM OF ION PUMPING IN BACTERIORHODOPSIN

Brian W. Edmonds [1] and Hartmut Luecke [1,2]

[1] *Department of Molecular Biology & Biochemistry,* [2] *Departments of Physiology & Biophysics, Information & Computer Science, University of California, Irvine, CA*

TABLE OF CONTENTS

1. ABSTRACT

A structure-based approach to the mechanism of ion pumping in bacteriorhodopsin (BR) has fostered new hypotheses for the detailed molecular changes that underlie ion transport in this light-driven pump. Isomerization of the retinal from all-*trans* to 13-*cis* in response to absorption of the energy of a photon is thought to lead to proton transfer from the initially protonated Schiff base to an anionic aspartate residue (Asp85) in the first half of the BR photocycle. In this traditional view the proton is transferred directly from the Schiff base to Asp85. A comparison of structures of photocycle intermediates trapped shortly after proton transfer to Asp85 to those of the resting state suggested an alternative view for the mechanism of proton transfer. In this scenario, a local water molecule in hydrogen bond contact with the Schiff base and Asp85 in the resting state is destabilized upon isomerization of the retinal. The destabilized water loses a proton to Asp85 and the remaining hydroxyl anion migrates toward the positively charged Schiff base to abstract its proton. This mechanism, in which a hydroxyl ion is pumped in lieu of a proton, has now been challenged by interpretations of new structures for photointermediates that immediately precede and follow the deprotonation/protonation reaction. However, in contrast to the older structures in which photointermediates were prepared at room temperature, the new structures were obtained by illuminating wild-type BR in frozen crystals. The results of spectroscopic studies of BR suggest that the structures of intermediates trapped at low temperature may not be the same as native photocycle intermediates at room temperature. The precise mechanism of ion transfer in BR is therefore unresolved.

2. INTRODUCTION

Bacteriorhodopsin is a 7-helical integral membrane protein of halophilic archaea that functions as a light-driven ion pump. As the best-understood protein of a structurally homologous family of photoactive rhodopsins, BR is a model for rhodopsins found in phylogenetically diverse microorganisms including haloarchaea, proteobacteria, cyanobacteria, fungi and algae (1-3). Members of one class of these microbial rhodopsins function as light-driven ion pumps. These include BR and halorhodopsin in haloarchaea and proteorhodopsins in marine bacteria. Rhodopsins of a second class, the sensory rhodopsins, include (phototactic) sensory rhodopsins I and II in haloarchaea (4, 5), *Chlamydomonas* rhodopsins CSRA and CSRB (3) and *Anabaena* rhodopsin (6).

Illumination of BR initiates a photocycle in which the energy of one photon is absorbed by a covalently bound retinal cofactor and used to drive the conformational changes that underlie ion pumping (7, 8). In the traditional view, BR pumps protons from the intracellular to the extracellular surface, generating an electrochemical gradient, which is then utilized by a second membrane protein, ATP synthase, for the production of intracellular ATP. For nearly 30 years, the focus of research on BR has been the mechanism of ion pumping, with recent focus on the structural underpinnings of functional properties assayed with biochemical, spectroscopic and electrophysiological methods. While many features of the mechanism have been clarified, a comprehensive description of the structural basis of ion translocation at the atomic level is lacking, due partly to uncertainty about the structural similarity between the normal photocycle intermediates and those prepared by "trapping" at low temperature or by the introduction of mutations that slow a particular photocycle reaction to accumulate an intermediate (9). Nevertheless, information from high-resolution crystal structures of BR in the resting state and in various intermediate states has motivated novel hypotheses for the mechanism of ion transport. In this review, we
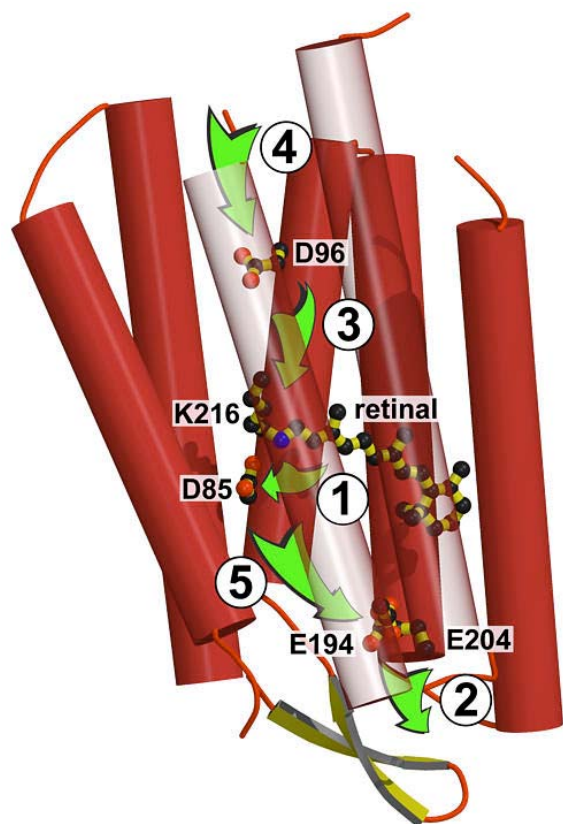
Figure 1. Overall view of bacteriorhodopsin, shown with the retinal and residues directly implicated in ion transport. Standard orientation with cytoplasmic side on top. The residues rendered explicitly are (from top to bottom): Asp96, all-*trans* retinal, Asp85, Arg82, Glu194/Glu204. The basic steps after the initial photon-driven all-*trans* to 13-*cis* retinal isomerization are: (1) deprotonation of the Schiff base, protonation of nearby Asp85, yielding the early M intermediate, coupled via downward movement of Arg82; (2) proton expulsion at the extracellular surface from the proton release group near Glu194/Glu204, yielding the late M intermediate; (3) deprotonation of Asp96 and reprotonation of the Schiff base, yielding the N intermediate; (4) reprotonation of Asp96 from the cytoplasmic surface, thermal reisomerization of the retinal to all-*trans*, yielding the O intermediate; (5) deprotonation of Asp85, reprotonation of the proton release group, regenerating the resting state.

discuss these structures and the extent to which they support or refute various hypotheses for the mechanism of ion pumping.

The overall architecture of BR is that of two half-channels, a cytoplasmic and an extracellular one, separated by a retinal chromophore with a Schiff base linkage to Lys216 of helix G (the seventh and last helix) near the middle of the bilayer (Figure 1). The extracellular half-channel is comprised of an extensive hydrogen-bonded network of ordered waters and protein residues. Protonation of Asp85, in the first half of the photocycle,

triggers disruption of the hydrogen-bonded network of waters, resulting in the movement and reorientation of the guanidinium group of Arg82 toward the extracellular proton release group (Glu204/Glu194/waters) whereupon a proton is released at the extracellular surface (Figure 2) (10-12). With the exception of the O intermediate (13), the arrangement of extracellular portions of the helices, and therefore the overall conformation of the extracellular half-channel, is relatively fixed throughout the photocycle.

In contrast, the cytoplasmic half-channel is predominantly hydrophobic and lacks a sufficient number of ordered waters or polar residues to provide a path for the ion from the proton donor, Asp96, to the Schiff base, or from the cytoplasmic surface to Asp96. Consequently, in the latter part of the photocycle, reprotonation of the Schiff base occurs only after opening of the cytoplasmic half-channel by movement of the cytoplasmic ends of helices F and G, allowing a chain of water molecules to form and provide a pathway for ion transfer (14, 15).

3. STRUCTURE OF THE RESTING STATE OF BACTERIORHODOPSIN

The configuration of the retinal in light-adapted BR is all-*trans*. This light-adapted state of BR will be referred to as the resting state (BR) in this review (sometimes also called the "ground state"). Structural studies of BR in the resting state at 1.9 Å (16) and at 1.55 Å (12) now give a detailed view of the conformation of the transmembrane portion of BR including the retinal in its binding pocket and the region surrounding the active site, formed by the positively charged retinylidene N, the negatively charged carboxylate side chains of Asp85 and Asp212, and a water bound tightly between these charged moieties. While retinal atoms in proximity to the active site undergo rearrangements upon photoactivation of BR, atoms of the β-ionone ring and most of the polyene chain are less mobile. In the resting state, these atoms are held in place by apposition to 12 residues including the side chain of Trp182 in close contact with the 13-methyl group of the retinal on the cytoplasmic side. The orientation of the extended retinal polyene is transverse (20.5° degrees to the plane of the bilayer; Figure 1), and the hydrogen atom of the Schiff base N-H charge dipole projects toward the extracellular region, donating a hydrogen bond to an ordered water (W402) that, in turn, donates hydrogen bonds to OD1 of Asp85, to be protonated in the L to M transition, and OD1 of Asp212, which is thought to remain ionized throughout the photocycle (with the possible exception of the O-to-BR transition) (Figure 2). In the resting state, W402 provides a polar environment for the positively charged Schiff base and the negatively charged carboxylate oxygens of the two aspartate residues, stabilizing the ionic state of these moieties. OD1 of Asp85 accepts a second hydrogen bond from W401, which is connected to the NH2 of Arg82 via W406 (which also donates a hydrogen bond to OD2 of Asp212). A second chain of hydrogen bonds connects OD1 of Asp212 to NH1 and NH2 of Arg82 via the phenolic OH of Tyr57 and W407. In the resting state, the carboxylate anions of Asp85 and Asp212 are stabilized further by accepting hydrogen bonds at their OD2s from the side chains of Thr89 and Tyr185, respectively.
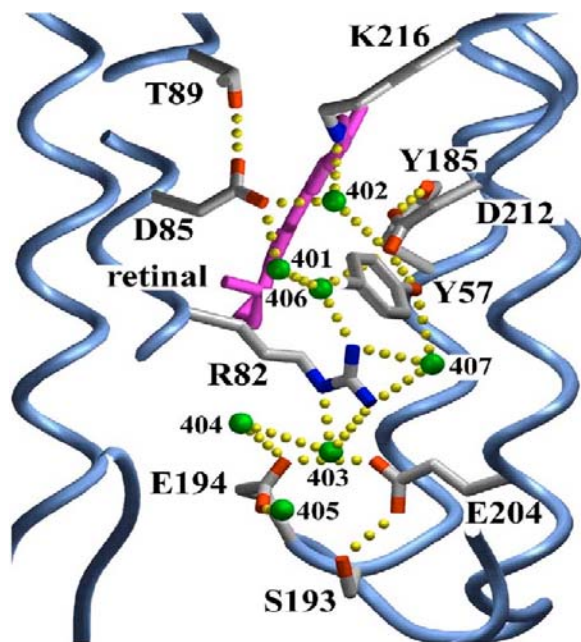
Figure 2. Illustration of the extracellular half-channel in the resting state with the hydrogen-bonded network of waters and key residues involved in ion transport. Lys216 and the attached retinal (purple) are shown in proximity to Asp85 and Asp212 forming the active site (together with W402). The active site is connected to Arg82 (via W401, W406, W407 and Tyr57), which in turn is connected to the proton release group (Glu194/Glu204/waters) and Ser193 near the extracellular surface. Ordered water molecules are shown in green.
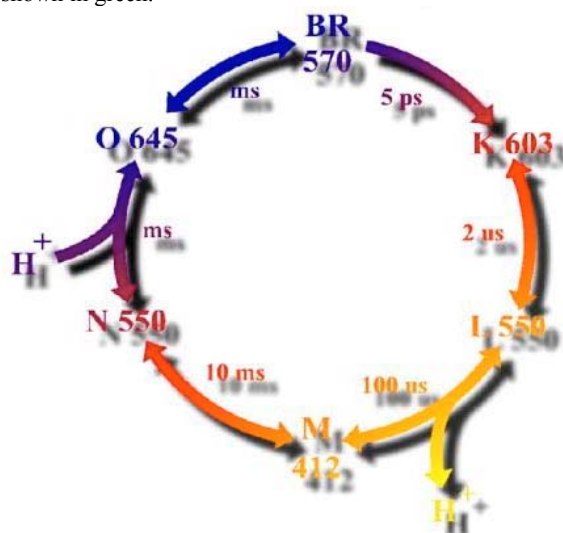
Figure 3. Illustration of the BR photocycle with the lifetimes of the photointermediates. Upon absorption of a photon, BR makes a transition to the J intermediate (not shown) in 0.5 ps. In the normal photocycle, a proton is expelled at the extracellular surface in late M, followed by proton uptake from the cytoplasmic surface to Asp96 in the N-to-O transition.

4. THE PHOTOCYCLE

The photocycle is initiated when the energy of a photon is absorbed by the retinal (λ_{max} 568 nm) to produce an isomerization around the $C_{13}=C_{14}$ double bond, converting the all-*trans* retinal of the resting state to a 13-*cis*,15-*anti* configuration. The first electronic ground state structure, J (λ_{max} 625 nm), is formed within 500 femtoseconds and it is likely that the configuration of the retinal is 13-*cis* by this time (17). The red-shifted K intermediate (λ_{max} 590 nm) is formed within 3 picoseconds (18, 19), and in the subsequent K → L and L → M transitions the energy of the photon, which is stored initially as distortions in the retinal, is progressively transferred to the protein. The net translocation of one ion across the bilayer is thus thermally driven via a series of structurally distinct intermediates (J, K, L, M, N and O) before the protein returns to the resting state (Figure 3).

Molecular rearrangements occurring near the active site upon formation and during the lifetime of the M state are of particular interest for the vectorial nature of ion transport in BR. The change in the protonation state of the Schiff base is the defining feature of the far blue-shifted M intermediate (λ_{max} 412 nm) which is subsequently red-shifted upon reprotonation of the Schiff base from the cytoplasmic side, corresponding to formation of the N intermediate (λ_{max} 560 nm). A change in the local environment of the Schiff base upon formation or during the lifetime of M is thought to be the basis for unidirectional pumping. Answers to three questions are of particular interest: 1) What is the orientation of the Schiff base N-H charge dipole in the L intermediate, just before deprotonation. 2) What drives deprotonation of the Schiff base in the L-to-M transition? 3) What are the molecular changes that ensure reprotonation of the Schiff base occurs from the cytoplasmic side (as opposed to futile reprotonation from Asp85) in the M-to-N transition? The first two questions could, in principle, be addressed by comparing high-resolution structures of the L and the earliest possible M state. Clues to the third question could come from the structures of sequential substates of M (see below). A related, unresolved issue is how to reconcile the apparent necessity of an influx of water molecules from the cytoplasmic side to facilitate reprotonation of the Schiff base from Asp96 with the requirement of preventing Asp96 from losing its proton to the cytoplasmic surface (Figure 1). The N-to-O transition is associated with reprotonation of Asp96 from the cytoplasmic side and thermal reisomerization of the retinal back to all-*trans*. In the final step back to the resting state (O-to-BR transition), Asp85 deprotonates and the proton release group in the extracellular channel is reprotonated.

5. NOMENCLATURE FOR SUBSTATES OF THE M INTERMEDIATE

An analysis of the kinetics of time-resolved visible spectra in response to a flash of actinic light suggested the existence of two distinct substates of M, denoted M1 and M2 (20). A later comparison of these kinetics at neutral pH, in which a proton is expelled at the extracellular surface, with those at low pH, in which proton
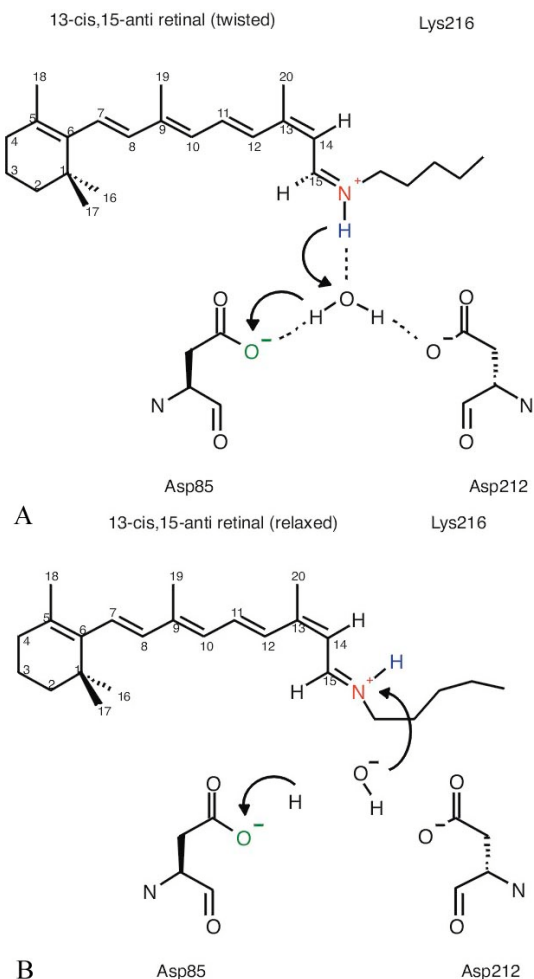
Figure 4. Schematics illustrating two distinct mechanisms for deprotonation of the Schiff base in the transition from L to M. A) A highly strained retinal in L would keep the Schiff base charge dipole oriented toward W402/Asp85/Asp212 on the extracellular side to allow transfer of the proton to Asp85 either directly (in the absence of W402) or, alternatively (if W402 is present), in a coordinated reaction via W402 (7). B) In this model for a net hydroxide ion pump, a relatively planar 13-*cis*,15-*anti* retinal with the Schiff base charge dipole oriented away from W402/Asp85/Asp212 and toward the hydrophobic cytoplasmic side would destabilize the two negatively charged carboxylates bridged by W402 (Asp85/Asp212), resulting in the abstraction of a proton from W402 by Asp85, generating a mobile hydroxide anion. The hydroxide anion would be repelled by the nearby anionic Asp212 and attracted toward the positively charged Schiff base on the cytoplasmic side of the chromophore. The hydrophobic environment of the cytoplasmic side would favor abstraction of the proton from the Schiff base by the basic hydroxide. It should be noted that net OH$^-$ transport across the bilayer into a cell can be achieved by proton transport in the outward direction, coupled to the transport of water molecules into the cell. Thus, most of the inferred proton transfer events of the bacteriorhodopsin photocycle could equally likely be part of a net hydroxide ion pumping mechanism.

release is inhibited, necessitated the addition of a third state, M2', to account for proton release (21). Thus, the spectral studies suggested the following scheme:

M1 ←→ M2 ←→ M2'.

There are now four high-resolution (2.0 Å or better) structures of M in the literature. The first two were obtained by populating the BR molecules in crystals of single-site mutants to the M intermediate to virtually 100% occupancy at room temperature, followed by cryo-trapping at 100 K (14, 15). The structure of the E204Q mutant, in which proton release on the extracellular side is blocked, was referred to as "early" M (15), to distinguish it from the "late" M (14) structure (D96N mutant), which accumulates because of inhibition of the transition to the N state, in which the Schiff base is reprotonated via Asp96. The third M intermediate was prepared by illumination of wild-type BR at 230 K, and because it is structurally similar to the E204Q intermediate, it will not be considered further (22). The correspondence between substates of M identified by spectroscopic methods and the x-ray structures of M is unclear (23); however, the simplest interpretation is that a recently published (fourth) low-temperature M intermediate (24), generated at 210 K and referred to here as M1$_{LT}$, resembles the early M state identified by time-resolved spectroscopy. The E204Q structure is a later M that may correspond to the spectroscopically defined M2. The M2' substate is probably well represented by the "late" D96N structure. The D96N photoproduct was originally classified as a fourth M state, M$_N$ (deprotonated Schiff base), because FTIR spectra indicated changes in protein bands normally observed only in the N state (25).

6. DEPROTONATION OF THE SCHIFF BASE

There are at least two classes of mechanisms that might explain the Schiff base deprotonation reaction in the L-to-M transition (7). In the first case, the L state is characterized by an orientation of the Schiff base N-H vector similar to that of the resting state, i.e. toward the extracellular side, with the Schiff base proton in proximity to OD1 of Asp85. In the L-to-M reaction the proton would then be transferred directly to Asp85 if W402 is absent in L, or, if W402 is still present in L, Asp85 would become protonated through a coordinated reaction in which the Schiff base proton is transferred to W402, coupled to transfer of one of its protons to Asp85 (Figure 4A). In the second scenario, the Schiff base proton in the L state is not in proximity to Asp85, and protonation of Asp85 occurs by another, less direct mechanism. For example, if the light-induced isomerization has reoriented the Schiff base N-H charge dipole from the hydrophilic extracellular to the hydrophobic cytoplasmic side in L, the ensuing electrostatic rearrangement could result in a destabilization of the charge triad NH$^+$/Asp85$^-$/Asp212$^-$. Asp85 could then abstract a proton from W402 and the resulting mobile hydroxide anion would be forced in the cytoplasmic direction as a result of repulsion by the anionic carboxylate of Asp212 on the extracellular side and attraction to the positively charged Schiff base on the cytoplasmic side, leading ultimately to abstraction of the Schiff base proton by the transient hydroxide ion (Figure 4B; see (7)). The main difference between these two mechanisms is that the

former requires a highly strained, twisted retinal in L in order to retain the Schiff base proton in proximity to Asp85 at the time of deprotonation, while destabilization of W402 in the latter mechanism would appear to require that the retinal adopts a more relaxed conformation that orients the Schiff base proton away from W402 and the extracellular side in general. For a relaxed retinal, direct transfer of the Schiff base proton would be precluded by the fact that proton transfers over distances of more than a few tenths of an Angstrom require carriers. It should be noted that if the retinal is in a relatively planar 13-*cis* conformation in K at room temperature (26) and the orientation of the N-H dipole is the main determinant of the stability of the $NH^+/Asp85^-/Asp212^-$ charge triad, then it is not clear why deprotonation of the Schiff base would not occur much earlier, for example in the transition from the J state. Nevertheless, transporting hydroxide anions toward the cytoplasmic side would make ion pumping in BR analogous to Cl^- ion pumping in halorhodopsin, which pumps Cl^- ions from the outside to the inside (27). That BR could function as a net hydroxide ion transporter is made more attractive by the fact that it can be converted into an inward Cl^- pump by mutation of Asp85 to either a serine or a threonine residue (28, 29) or, alternatively, by protonation of Asp85 at low pH (30). While the configuration of the retinal is not likely to be the only relevant factor for the mechanism of deprotonation, the orientation of the N-H vector in L, just prior to deprotonation of the Schiff base, is of considerable interest.

Inferences about the mechanism of ion pumping made from trapped intermediates in crystallographic studies require that these intermediates are not dissimilar to the native intermediates formed during the normal photocycle at ambient temperature, and also that little ambiguity is introduced into the proposed mechanism due to lack of information about the transition pathways between the states. Otherwise, inferences made from structures are likely to be of limited use. The structures of all BR photointermediates would ideally be determined in the native environment of the purple membrane as trapped wild-type species produced at ambient temperature. In addition to the potential confounding effects of trapping intermediates by illumination at low temperature or by mutation of the wild-type protein, other factors may introduce significant structural alterations not characteristic of the normally occurring intermediates, including solubilization of the protein in detergent, artificial packing of the protein in 3-D crystals, and x-radiation damage during data collection (31). Most of the structures of photointermediates discussed here were obtained from 3-D crystals grown in cubic lipid phase (32). The fact that BR exhibits largely normal photocycle kinetics at room temperature in these 3-D crystals (33) suggests that neither detergent extraction nor stacking of bilayers in the 3-D matrix significantly distorts the wild-type BR photocycle.

7. INTERMEDIATES PREPARED AT LOW TEMPERATURE MAY BE DIFFERENT FROM NORMAL PHOTOCYCLE INTERMEDIATES

To obtain crystal structures of photocycle intermediates, a population of BR molecules must be arrested or trapped, ideally, in just one of the meta-stable intermediate states at 100% occupancy. Typically, either a mutation is introduced to slow down a particular photocycle reaction at room temperature and accumulate an intermediate (9) or, alternatively, certain intermediate states (usually K, L or early M) are populated by photoactivation at low temperature (34). In the latter case, the photointermediate of interest cannot be populated to full occupancy because its spectrum overlaps those of other intermediates and that of the resting state.

The first intermediate of the photocycle for which a "trapping" method exists is K. Therefore neither the electronically excited state intermediates, H and I, that exist transiently (lifetimes < 500 fs) following photoactivation, nor the vibrationally hot electronic ground state intermediate J, the immediate precursor to K, have been studied using crystallographic methods. Some structural information of the early J intermediate has, however, been obtained with time-resolved spectroscopic methods. These methods probe the configuration (for example, 13-*cis* vs. 13-*trans*) and conformation (for example, relaxed/planar vs. strained/twisted) of the retinal at room temperature. Time-resolved spectroscopic methods have also been used to investigate the structure of the chromophore in the K and L intermediates, which so far have been prepared for crystallographic studies only by trapping at low temperature.

At room temperature, the first electronic ground state intermediate is J (18, 35, 36). A time-resolved Raman spectroscopy study of BR (26) and a time-resolved absorption and fluorescence study of BR with a locked retinal, in which isomerization of the $C_{13}=C_{14}$ double bond was prevented by chemical modification (37), suggest that J is a vibrationally "hot" photoproduct with a strained, twisted retinal. A recent infrared spectroscopic study with femtosecond resolution suggests that the retinal is isomerized to 13-*cis* in J (17); however, there remains disagreement on this issue (38). Significantly, the conformation of the 13-*cis* retinal in K (formed within 3 picoseconds) at room temperature is nearly planar, only to become twisted again in late K (26, 39). In contrast, when K is prepared at low temperature (77 K, denoted as K_{LT}), the hydrogen-out-of-plane (HOOP) region of the Raman spectrum (850-1050 cm^{-1}) is characteristic of a twisted chromophore (40). It is therefore possible that at cryogenic temperature the protein matrix housing the retinal is non-compliant and blocks, delays or alters the normal J-to-K transition occurring at room temperature. Regardless, the conformation of the retinal in K_{LT} does not resemble that of any of the subset of spectroscopically identified K intermediates observed in the normal photocycle at room temperature (41).

Step-scan FTIR studies also suggest that the geometry of the chromophore in L at room temperature is different from that of L prepared at low temperature (denoted L_{LT}) (42, 43). For example, the 15-H HOOP mode at 983 cm^{-1} in the L state at room temperature is not present in L_{LT} (43), although it should be noted that in this case the effect of the presumably less compliant low temperature condition is opposite to that on the K

intermediate. Moreover, a chromophore band at 1155 cm^{-1}, indicative of a the C_{14}-C_{15} stretching vibration, is present in L_{LT} (44), but not observed in room temperature L-M difference spectra (43).

8. STRUCTURE OF THE LOW-TEMPERATURE K INTERMEDIATE

In spite of the fact that neither K_{LT} nor L_{LT} are likely to resemble K (26, 41) or L (42, 43), respectively, at room temperature, we will consider structures of K_{LT} and L_{LT} to determine what they might suggest about the sequence of events leading to deprotonation of the Schiff base in the L-to-M transition. There are now two high-resolution structures for K_{LT}, both refined allowing two simultaneous alternate conformations, one for the resting state fraction of the crystal and one for the K_{LT} fraction (45, 46). The first structure with 35% K_{LT} occupancy at 2.1 Å indicated changes that were not restricted to the retinal, including dislocation of W402 and a movement of Asp85 toward the position occupied by the Schiff base in the resting state (45). Unfortunately, the limited resolution in combination with low partial occupancy was not sufficient to refine the retinal of K_{LT} free from bias caused by stereochemical restraints, and thus it was simply modeled in a planar, 13-*cis*,15-*anti* conformation (45).

The structure of K_{LT} was recently reexamined at higher resolution (1.43 Å), albeit from merohedrally twinned crystals, without retinal planarity or other stereochemical restraints (46) by photoactivation at 100 K to produce a mixture of 60% BR and 40% K_{LT} as estimated from difference spectra. In stark contrast to the earlier K_{LT} structure, both W402 and Asp85 remain in their resting state positions. Structural differences are largely restricted to the retinal, which is in an extended, and therefore strained 13-*cis*,15-*anti* conformation. The C_{13}=C_{14} torsion angle is fully rotated from *trans* to *cis*; however, the retinal remains extended, rather than adopting the expected kinked conformation. The model-based refinement employed in this study suggests that the resulting strain is focused in a single bond angle, a significantly increased C_{12}–C_{13}=C_{14} angle, and in counter-rotations of the two covalent bonds between C_{14} and NZ. The position of the Schiff base nitrogen is unchanged in this K_{LT}; however, the NZ–H$^{...}$O hydrogen bond angle to W402 is reduced by about 30° relative to the resting state, suggesting that this hydrogen bond is weakened significantly or even lost. Nevertheless, the Schiff base proton has not oriented toward the cytoplasmic side due to counter-rotations around C_{14}–C_{15} and, to a larger extent, around C_{15}=NZ. Weakening of the hydrogen bond between the Schiff base and W402 is proposed to manifest itself as a destabilization of the entire hydrogen bonded network in the extracellular channel (46). This network, linking the active site to Arg82, is disrupted in mid- to late M (15).

The means of free energy storage in K_{LT} has been hypothesized to reside primarily in distortion of retinal bond and torsion angles that arise from steric conflict between the retinal and surrounding protein residues (47, 48). Alternatively, the increased free energy could arise from either a simple charge separation of the positively charged Schiff base nitrogen and its complex counterion (Asp85/Asp212/waters) (38, 49, 50), or from a reorientation of the N–H charge dipole of the Schiff base from the very polar environment of the extracellular half-channel to the hydrophobic environment of the cytoplasmic half-channel (7). Given that the Schiff base nitrogen moves less than 0.2 Å in K_{LT} and given the relatively small change in the N-H vector orientation, the more recent K_{LT} structure favors the interpretation that the free energy is stored as retinal distortions, particularly the bond angle at C_{13} and the counter-rotation of the C_{15}=NZ bond. The twisted conformation is consistent with an FTIR study indicating that the dipole moment of the N-H stretch is approximately 90° to the membrane normal in K_{LT} (51). The sites of energy storage in K_{LT} may therefore be different from those of K prepared at room temperature. In the latter case, the energy is thought to reside in both the altered electrostatic interaction between the Schiff base charge dipole and the complex counterion (Asp85/Asp212/waters) and the steric interactions that arise from a near planar 13-*cis* retinal, with in-plane bond angle strains, in an all-trans pocket (26). Thus, it appears unlikely that the twisted retinal observed in the low-temperature, 1.43 Å structure for K_{LT} resembles the retinal in K at room temperature.

9. STRUCTURE OF THE LOW-TEMPERATURE L INTERMEDIATE

Evolution of the K state structure to produce a deprotonated Schiff base in M requires the formation of the L intermediate. There is a low temperature 2.1 Å structure for L (denoted L_{LT}) derived from partially occupied crystals (52); however, at this resolution the unavoidable contamination of L (36%) with BR (40%), K (12%) and M (12%) (53) makes it difficult to ascertain which features of the structure are associated with L_{LT} (34, 53, 54). Nevertheless, in this L_{LT} the hydrogen-bonded network of waters in the extracellular region appears disrupted (W402 is absent), and the resulting enhancement of the electrostatic interaction between Asp85 and the positively charged Schiff base causes flexion of helix C toward the long axis of the channel (52). It was argued that flexion of helix C would reduce the distance between carboxylate atoms of Asp85 the Schiff base, thereby facilitating direct proton transfer (52). The suggested approach of Asp85 toward the Schiff base would be consistent with NMR studies showing an enhanced interaction (relative to the BR state) between the protonated Schiff base and its counterion in L_{LT} (55). Unfortunately, a recent reanalysis of the coordinate set for the 2.1 Å L_{LT} (1E0P) suggests that the distances between NZ and the carboxylate atoms (CA, OD1 and OD2) are not different from those of the resting state (56).

A second, higher resolution (1.62 Å) structure for L_{LT} was reported recently (56). This L intermediate was prepared to 60% occupancy by red laser illumination at 170 K. Unlike the previous structure for L_{LT}, this structure is free of contamination from K but still contains 10% M (56). In stark contrast to the earlier 2.1 Å L_{LT} structure, the network of waters in the extracellular channel, including W402, are intact, and a medial shift of the carboxylate atoms of Asp85 (flexion of helix C) was not observed (56). The most interesting features of the 1.62 Å structure of L_{LT} are best described relative to the 1.43 Å structure for K_{LT}

reported by the same group (46). The extended C_{12}–C_{13}=C_{14} angle in K_{LT} remains extended, and therefore strained, in L_{LT} (56). The torsion angles of the C_{13}=C_{14} and C_{15}=NZ double bonds are counterrotated in L_{LT} relative to their angles in K_{LT} (56). Thus, the N-H vector has re-oriented toward the extracellular side, and the NZ–H··O hydrogen bond angle, which deviated from the resting state value by 30° in K_{LT}, is within 10° of the resting state value in this L_{LT} (56). The hydrogen bond from the Schiff base to W402, weakened in K_{LT}, may therefore be strengthened in L_{LT}.

10. STRUCTURE OF THE LOW-TEMPERATURE EARLY M INTERMEDIATE

The first intermediate structure of BR was that of the late M ($M2'/M_N$) state, determined at 100% occupancy using the D96N mutant (14). This was followed with an earlier M (M2) state using the E204Q mutant, also at full occupancy (15). Both of these M intermediates were produced by illumination at ambient temperature, followed by cryo-trapping at 100 K. While production of intermediates at ambient temperature and at full occupancy is clearly an advantage over low-temperature illumination schemes and partial occupancies, the use of single-site mutants, even when only involving conservative amino acid changes, warrants some caution due to the structural changes stemming from the mutation. These changes are usually restricted to the immediate vicinity of the mutation and are largely a result of the different hydrogen bonding geometries of protonated carboxylates vs. amides. For both the M2 (E204Q) and M2' (D96N) structures, W402 is notably absent. Moreover, the electron pair of the retinylidene nitrogen has already reoriented (albeit incompletely) toward the cytoplasmic side in M2, and by M2' the reorientation is complete (14, 15).

An early M state structure prepared from wild-type BR by illumination at 210 K refined with 60% occupancy was published recently (24). This 1.43 Å structure, also obtained by model-based refinement and referred to as $M1_{LT}$ here, is thought to represent an earlier M state than those of the E204Q (M2) and D96N (M2') mutants. Unlike the later M structures, W402 is present in $M1_{LT}$. Also, in $M1_{LT}$ the torsion angles for bonds between C_{13} and NZ are close to the values reported for K_{LT} (46), which keeps the deprotonated Schiff base oriented toward the extracellular side. In the E204Q structure (15), the torsion angles between C_{13} and NZ are relaxed such that the C_{15}=NZ-CE bond angle now points toward the cytoplasmic side, suggesting that the orientation of the Schiff base may change in the M1-to-M2 transition.

While the conformation of the retinal is similar in K_{LT} (1.43 Å), L_{LT} (1.62 Å) and $M1_{LT}$, the environment of the extracellular half-channel has changed. The hydrogen bond between NZ of the now deprotonated Schiff base and W402 is lost in $M1_{LT}$ and W402 is 0.9 Å further from the Schiff base as compared to the resting state (24). The remainder of the hydrogen bonded network in the region of Asp85 and Asp212 (W402, W401 and W406) is still intact; however, W406 has lost its bond to NH2 of Arg82 and W407, which links Tyr57 to NH1 and NH2 of Arg82 in the

resting state, is now only weakly bonded to Tyr57. Arg82, which has moved toward the proton release group in the later E204Q structure for M, has not yet moved from its resting state position.

One mechanism for deprotonation, introduced above, posits that the protonated Schiff base charge dipole points toward the cytoplasmic side in late L (7). The ensuing electrostatic destabilization of the region of the two anionic groups on the extracellular side, Asp85 and Asp212, results in the dissociation of interposed W402 into a proton that neutralizes the charge of one of the two nearby carboxylates, that of Asp85, and a mobile hydroxide anion that would now be repelled by nearby Asp212 which remains anionic. In addition, this hydroxide ion would be attracted by the positively charged Schiff base on the cytoplasmic side, immediately abstracting the Schiff base proton once it reached the cytoplasmic side in the L-to-M transition. The orientation of the Schiff base in the $M1_{LT}$ structure (extracellular) and the presence of W402 (in $M1_{LT}$) are inconsistent with this mechanism. The structure of partially occupied $M1_{LT}$ favors a scenario in which the Schiff base proton is transferred, either directly or via W402, to Asp85.

11. B-FACTORS AND THE 1.43 Å STRUCTURES FOR K_{LT} AND $M1_{LT}$

Crystallographic refinement typically yields Cartesian 3-D coordinates and an isotropic temperature factor (B-factor) that reflects the static and dynamic disorder for each atom. The B-factor is therefore correlated with the dynamic motion of an atom such that tightly packed core atoms and loosely packed surface atoms tend to have low and high B-factors, respectively. Moreover, the B-factors of bonded, and to a slightly lesser extent, of non-bonded neighboring atoms are correlated (57, 58), and crystallographic refinement programs typically restrain the B-factors of atoms connected by a bond. Table 1 lists B-factors for atoms at the active site for two high-resolution structures of the resting state (1C3W and 1M0L) as well as those of the partially occupied conformations of the K_{LT} (1M0K) and $M1_{LT}$ (1M0M) structures. For the resting state structures, refined at 100% occupancy, the B-factors of these bonded atoms are clearly correlated. NZ of the Schiff base, W402 and the atoms of the terminal portions of the nearby carboxylate side chains (CG, OD1 and OD2) of Asp85 and Asp212 all have similar values for the B-factor. In contrast, for the 40% occupied K_{LT} intermediate (1M0K_.4), the B-factor for W402 (39.85 Å^2) is approximately twice the value of the surrounding NZ and carboxylate atoms, which range from 16.14 to 20.48 Å^2. The B-factors for W401 and W406 are also high, whereas the B-factor for W402 in the resting state conformation (24.46 Å^2; 1M0K_.6) is more in line with the surrounding atoms. One explanation for this unusual lack of B factor correlation might be that W402 has significantly increased mobility in K_{LT}. However, the structural changes (in comparison to BR) in this densely packed active site do not suggest an increased volume for W402 to occupy. Alternatively, an overestimation of its relative occupancy would yield a B-factor that is artificially high (the crystallographic refinement program compensates excess

Table 1. B-factors for active site atoms of bacteriorhodopsin for the resting state and for the low-temperature intermediates K_{LT} and $M1_{LT}$

Resolution				D85			D212				
		NZ	W402	CG	OD1	OD2	CG	OD1	OD2	W401	W406
1C3W	1.55	23.55	26.50	21.13	20.29	24.50	17.27	22.84	19.45	23.11	26.49
1M0L	1.47	21.20	22.49	16.01	17.82	19.08	15.59	20.19	18.86	20.38	26.22
1M0K_.6		21.07	24.46	16.99	17.09	18.79	16.14	18.38	19.01	20.19	25.79
1M0K_.4	1.43	20.48	39.85	17.13	17.03	18.55	16.14	18.38	19.01	34.60	41.87
1M0M_.4		23.11	22.16	16.53	41.15	30.24	17.13	18.89	32.40	20.51	27.41
1M0M_.6	1.43	24.79	36.68	21.21	20.36	24.10	18.69	17.44	13.36	36.72	22.24

B-factors for atoms at the active site for two high-resolution structures of the resting state (1C3W and 1M0L) and for two structures of mixed occupancy (resting state and intermediates) K_{LT} (1M0K) and $M1_{LT}$ (1M0M). For the resting state structures, refined at 100% occupancy, the B-factors of these atoms are clearly correlated. NZ of the Schiff base, W402 and the atoms of the terminal portions of the nearby carboxylate side chains (CG, OD1 and OD2) of Asp85 and Asp212 all have similar values for the B-factor. In contrast, for the 40% occupied K_{LT} intermediate (1M0K_.4), the B-factor for W402 (39.85 Å^2) is approximately twice the value of the surrounding NZ and carboxylate atoms, which range from 16.14 to 20.48 Å^2. The B-factors for W401 and W406 are also high, whereas the B-factor for W402 in the resting state (60% BR, 1M0K_.6) is much lower (24.46 Å^2). For the illuminated conformation of $M1_{LT}$ (1M0M_.6) the value for W402 (36.68 Å^2) is also high relative to those of the other active site atoms, which range from 13.36 to 24.10 Å^2 (NZ is not included since it is no longer in hydrogen bond contact with W402 in the M state).
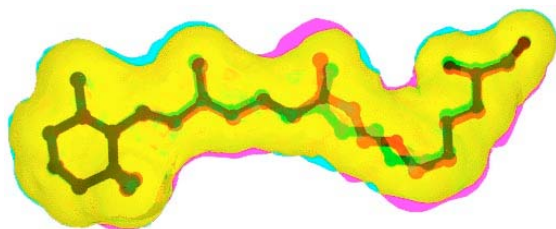
Figure 5. Illustration of the similarity in shape (and electron density) of the all-*trans* and the 13-*cis*,15-*anti* configurations of the retinal. Both retinal configurations were taken from the PDB file 1QKP (45), which describes a 2.1 Å resolution structure of a low-temperature K_{LT} intermediate of bacteriorhodopsin. The intermediate is reported at 35% occupancy, spatially overlapping with the remaining 65% constituting the resting state. In this figure the molecular envelope of the light-isomerized 13-*cis*,15-*anti* K_{LT} state is overlaid with that of the all-*trans* resting state, both shown with the covalently attached Lys216. Yellow depicts regions where both envelopes overlap, blue depicts regions occupied only by the all-*trans* isomer, and magenta depicts regions occupied only by the 13-*cis*,15-*anti* isomer. This figure was produced with the programs Swiss-PdbViewer (61) and POV-Ray version 3.1g (http://www.povray.org/).

model electrons by raising the B-factor to effectively smear them out). Therefore, it is possible that the occupancy of W402 (and perhaps of W401 and W406) in K_{LT} is not 100% of the photoproduct as modeled. It is also unclear why B-factors (and coordinates) of the Asp212 side chain of the resting state and activated state were not refined independently.

The B-factor data for the illuminated 60% $M1_{LT}$ (1M0M_.6) and 40% resting state (1M0M_.4) structures of 1M0M are also difficult to explain (Table 1). The value for W402 (36.68 Å^2) in the illuminated conformation (1M0M_.6) is also very high relative to those of the other active site atoms, which range from 13.36 to 21.21 Å^2 (NZ is not included since it is no longer in hydrogen bond contact with W402 in the M state). Assuming W402 is

fully occupied in the illuminated state, the data suggest that it is highly mobile relative to the coordinating oxygens of the nearby aspartate side chains. This is perhaps not entirely surprising given that W402 is no longer accepting a hydrogen bond from NZ. Interestingly, for the resting state conformation of 1M0M, the B-factor for W402 is similar to those of other resting state structures (e.g., 1C3W and 1M0L), whereas the B-factor for OD1 of Asp85, to which W402 is hydrogen bonded, is aberrantly high. The reason for this pattern is unclear, but it suggests that caution is warranted when attributing significance to the precise location of active site atoms under conditions of merohedral twinning (59), partial occupancy, nearly complete spatial overlap (Figure 5) and model-based refinement.

12. SUMMARY AND PERSPECTIVE

Inferences about the mechanisms underlying ion transport in BR from structural data depend critically on the ability to trap a relatively pure population of molecules in a given meta-stable state, and the structures of these intermediates must bear a close resemblance to the room temperature (native) intermediate in wild-type BR. In many instances, methods for preparing a pure sample (100% occupancy) are not available, and this is a significant problem for studies of the early J, K and L intermediates of the BR photocycle. Features of the electron density that arise from contaminating intermediates or the resting state may be particularly difficult to recognize and therefore lead to errors in modeling and refinement. Even in cases where spectroscopic analyses of the visible absorbance maximum of the crystal indicate that a population of protein molecules is structurally homogeneous, one cannot be certain that the population is structurally pure. While visible light spectroscopy is useful in identifying various intermediates, it may not always be diagnostic. It is well known that some transitions in the BR photocycle are spectrally silent. The spectra of the various M substates, for example, do not show large differences in their absorption maxima, despite significant changes in the active site. It is also thought that the resting state of BR

may be contaminated by other intermediates (*pseudo*-BR and *iso*-BR), for example, when attempting to produce the K_{LT} intermediate with high-intensity illumination (34), and the K intermediate itself may contain several substates (60). The problem of identifying these contaminating photoproducts exacerbates the difficulties when refining structures at partial occupancy, particularly when the expected structural changes are very small and spatially overlapping. The problem is illustrated in Figure 5 which depicts an overlay of the molecular envelopes for the all-*trans* and 13-*cis*,15-*anti* configurations of the retinal. Differences in the electron density are surprisingly minor. Finally, trapping methods that do not yield pure samples (as well as those that do) may also yield structurally deviant photoproducts. The recent publication of several high-resolution structures of BR intermediates has fueled many hypotheses regarding the mechanisms contributing to ion transport in BR; however, many basic questions remain unanswered.

13. ACKNOWLEDGEMENT

14. REFERENCES

1. Spudich, J.L., C.S. Yang, K.H. Jung & E.N. Spudich: Retinylidene proteins: structures and functions from archaea to humans. *Annu Rev Cell Dev Biol* 16, 365-392 (2000)

2. Beja, O., E.N. Spudich, J.L. Spudich, M. Leclerc & E.F. DeLong: Proteorhodopsin phototrophy in the ocean. *Nature* 411 (6839), 786-789 (2001)

3. Sineshchekov, O.A., K.H. Jung & J.L. Spudich: Two rhodopsins mediate phototaxis to low- and high-intensity light in Chlamydomonas reinhardtii. *Proc Natl Acad Sci U S A* 99 (13), 8689-8694 (2002)

4. Hoff, W.D., K.H. Jung & J.L. Spudich: Molecular mechanism of photosignaling by archaeal sensory rhodopsins. *Annu Rev Biophys Biomol Struct* 26, 223-258 (1997)

5. Spudich, J.L. & H. Luecke: Sensory rhodopsin II: functional insights from structure. *Curr Opin Struct Biol* 12 (4), 540-546 (2002)

6. Jung, K.H., V.D. Trivedi & J.L. Spudich: Demonstration of a sensory rhodopsin in eubacteria. *Mol Microbiol* 47 (6), 1513-1522 (2003)

7. Luecke, H.: Atomic resolution structures of bacteriorhodopsin photocycle intermediates: the role of discrete water molecules in the function of this light-driven ion pump. *Biochim Biophys Acta* 1460 (1), 133-156 (2000)

8. Pebay-Peyroula, E., R. Neutze & E.M. Landau: Lipidic cubic phase crystallization of bacteriorhodopsin and cryotrapping of intermediates: towards resolving a revolving photocycle. *Biochim Biophys Acta* 1460 (1), 119-132 (2000)

9. Brown, L.S.: Reconciling crystallography and mutagenesis: a synthetic approach to the creation of a comprehensive model for proton pumping by bacteriorhodopsin. *Biochim Biophys Acta* 1460 (1), 49-59 (2000)

10. Balashov, S.P., E.S. Imasheva, R. Govindjee & T.G. Ebrey: Titration of aspartate-85 in bacteriorhodopsin: what it says about chromophore isomerization and proton release. *Biophys J* 70 (1), 473-481 (1996)

11. Richter, H.T., L.S. Brown, R. Needleman & J.K. Lanyi: A linkage of the pKa's of asp-85 and glu-204 forms part of the reprotonation switch of bacteriorhodopsin. *Biochemistry* 35 (13), 4054-4062 (1996)

12. Luecke, H., B. Schobert, H.T. Richter, J.P. Cartailler & J.K. Lanyi: Structure of bacteriorhodopsin at 1.55 Å resolution. *J Mol Biol* 291 (4), 899-911 (1999)

13. Rouhani, S., J.P. Cartailler, M.T. Facciotti, P. Walian, R. Needleman, J.K. Lanyi, R.M. Glaeser & H. Luecke: Crystal structure of the D85S mutant of bacteriorhodopsin: model of an O-like photocycle intermediate. *J Mol Biol* 313 (3), 615-628 (2001)

14. Luecke, H., B. Schobert, H.T. Richter, J.P. Cartailler & J.K. Lanyi: Structural changes in bacteriorhodopsin during ion transport at 2 angstrom resolution. *Science* 286 (5438), 255-261 (1999)

15. Luecke, H., B. Schobert, J.P. Cartailler, H.T. Richter, A. Rosengarth, R. Needleman & J.K. Lanyi: Coupling photoisomerization of retinal to directional transport in bacteriorhodopsin. *J Mol Biol* 300 (5), 1237-1255 (2000)

16. Belrhali, H., P. Nollert, A. Royant, C. Menzel, J.P. Rosenbusch, E.M. Landau & E. Pebay-Peyroula: Protein, lipid and water organization in bacteriorhodopsin crystals: a molecular view of the purple membrane at 1.9 Å resolution. *Structure Fold Des* 7 (8), 909-917 (1999)

17. Herbst, J., K. Heyne & R. Diller: Femtosecond infrared spectroscopy of bacteriorhodopsin chromophore isomerization. *Science* 297 (5582), 822-825 (2002)

18. Sharkov, A.V., A. Matveets Iu, S.V. Chekalin & A.V. Pakulev: Subpicosecond spectroscopy of bacteriorhodopsin. *Dokl Akad Nauk SSSR* 281 (2), 466-470 (1985)

19. Polland, H.J., M.A. Franz, W. Zinth, W. Kaiser, P. Hegemann & D. Oesterhelt: Picosecond events in the photochemical cycle of the light-driven chloride-pump halorhodopsin. *Biophys J* 47 (1), 55-59 (1985)

20. Varo, G. & J.K. Lanyi: Kinetic and spectroscopic evidence for an irreversible step between deprotonation and reprotonation of the Schiff base in the bacteriorhodopsin photocycle. *Biochemistry* 30 (20), 5008-5015 (1991)

21. Zimanyi, L., G. Varo, M. Chang, B. Ni, R. Needleman & J.K. Lanyi: Pathways of proton release in the bacteriorhodopsin photocycle. *Biochemistry* 31 (36), 8535-8543 (1992)

22. Facciotti, M.T., S. Rouhani, F.T. Burkard, F.M. Betancourt, K.H. Downing, R.B. Rose, G. McDermott & R.M. Glaeser: Structure of an early intermediate in the M-state phase of the bacteriorhodopsin photocycle. *Biophys J* 81 (6), 3442-3455 (2001)

23. Betancourt, F.M. & R.M. Glaeser: Chemical and physical evidence for multiple functional steps comprising the M state of the bacteriorhodopsin photocycle. *Biochim Biophys Acta* 1460 (1), 106-118 (2000)

24. Lanyi, J. & B. Schobert: Crystallographic structure of the retinal and the protein after deprotonation of the Schiff base: the switch in the bacteriorhodopsin photocycle. *J Mol Biol* 321 (4), 727-737 (2002)

25. Sasaki, J., Y. Shichida, J.K. Lanyi & A. Maeda: Protein changes associated with reprotonation of the Schiff base in the photocycle of Asp96-->Asn bacteriorhodopsin.

The MN intermediate with unprotonated Schiff base but N-like protein structure. *J Biol Chem* 267 (29), 20782-20786 (1992)

26. Doig, S.J., P.J. Reid & R.A. Mathies: Picosecond time-resolved resonance Raman spectroscopy of bacteriorhodopsin's J, K, and KL intermediates. *J Phys Chem* 95 (16), 6372-6379 (1991)

27. Kolbe, M., H. Besir, L.O. Essen & D. Oesterhelt: Structure of the light-driven chloride pump halorhodopsin at 1.8 Å resolution. *Science* 288 (5470), 1390-1396 (2000)

28. Brown, L.S., R. Needleman & J.K. Lanyi: Interaction of proton and chloride transfer pathways in recombinant bacteriorhodopsin with chloride transport activity: implications for the chloride translocation mechanism. *Biochemistry* 35 (50), 16048-16054 (1996)

29. Sasaki, J., L.S. Brown, Y.S. Chon, H. Kandori, A. Maeda, R. Needleman & J.K. Lanyi: Conversion of bacteriorhodopsin into a chloride ion pump. *Science* 269 (5220), 73-75 (1995)

30. Kalaidzidis, I.V. & A.D. Kaulen: Cl- -dependent photovoltage responses of bacteriorhodopsin: comparison of the D85T and D85S mutants and wild-type acid purple form. *FEBS Lett* 418 (3), 239-242 (1997)

31. Matsui, Y., K. Sakai, M. Murakami, Y. Shiro, S. Adachi, H. Okumura & T. Kouyama: Specific damage induced by x-ray radiation and structural changes in the primary photoreaction of bacteriorhodopsin. *J Mol Biol* 324 (3), 469-481 (2002)

32. Landau, E.M. & J.P. Rosenbusch: Lipidic cubic phases: a novel concept for the crystallization of membrane proteins. *Proc Natl Acad Sci U S A* 93 (25), 14532-14535 (1996)

33. Heberle, J., G. Buldt, E. Koglin, J.P. Rosenbusch & E.M. Landau: Assessing the functionality of a membrane protein in a three- dimensional crystal. *J Mol Biol* 281 (4), 587-592 (1998)

34. Balashov, S.P. & T.G. Ebrey: Trapping and spectroscopic identification of the photointermediates of bacteriorhodopsin at low temperatures. *Photochem Photobiol* 73 (5), 453-462 (2001)

35. Mathies, R.A., C.H. Brito Cruz, W.T. Pollard & C.V. Shank: Direct observation of the femtosecond excited-state *cis-trans* isomerization in bacteriorhodopsin. *Science* 240 (4853), 777-779 (1988)

36. Dobler, J., W. Zinth, W. Kaiser & D. Oesterhelt: Excited-state reaction dynamics of bacteriorhodopsin studied by femtosecond spectroscopy. *Chem Phys Lett* 144, 215-220 (1988)

37. Delaney, J.K., T.L. Brack, G.H. Atkinson, M. Ottolenghi, G. Steinberg & M. Sheves: Primary picosecond molecular events in the photoreaction of the BR5.12 artificial bacteriorhodopsin pigment. *Proc Natl Acad Sci U S A* 92 (6), 2101-2105 (1995)

38. Atkinson, G.H., L. Ujj & Y. Zhou: Vibrational spectrum of the J-625 intermediate in the room temperature bacteriorhodopsin photocycle. *J Phys Chem A* 104, 4130 (2000)

39. Mathies, R.A., S.W. Lin, J.B. Ames & W.T. Pollard: From femtoseconds to biology: mechanism of bacteriorhodopsin's light-driven proton pump. *Annu Rev Biophys Biophys Chem* 20, 491-518 (1991)

40. Braiman, M. & R. Mathies: Resonance Raman spectra of bacteriorhodopsin's primary photoproduct: evidence for a distorted 13-*cis* retinal chromophore. *Proc Natl Acad Sci U S A* 79 (2), 403-407 (1982)

41. Dioumaev, A.K. & M. Braiman: Two bathointermediates of the bacteriorhodopsin photocycle, distinguished by nanosecond time-resolved FTIR spectroscopy at room temperature. *J Phys Chem B* 101, 1655-1662 (1997)

42. Hage, W., M. Kim, H. Frei & R. Mathies: Protein dynamics in the bacteriorhodopsin photocycle: a nanosecond step-scan FTIR investigation of the KL to L transition. *Journal of Physical Chemistry* 100 (39), 16026-16033 (1996)

43. Rodig, C., I. Chizhov, O. Weidlich & F. Siebert: Time-resolved step-scan Fourier transform infrared spectroscopy reveals differences between early and late M intermediates of bacteriorhodopsin. *Biophys J* 76 (5), 2687-2701 (1999)

44. Gerwert, K. & F. Siebert: Evidence for light-induced 13-*cis*,14-*s-cis* isomerization in bacteriorhodopsin obtained by FTIR difference spectroscopy using isotopically labelled retinals. *Embo J* 5, 805-811 (1986)

45. Edman, K., P. Nollert, A. Royant, H. Belrhali, E. Pebay-Peyroula, J. Hajdu, R. Neutze & E.M. Landau: High-resolution X-ray structure of an early intermediate in the bacteriorhodopsin photocycle. *Nature* 401 (6755), 822-826 (1999)

46. Schobert, B., J. Cupp-Vickery, V. Hornak, S. Smith & J. Lanyi: Crystallographic structure of the K intermediate of bacteriorhodopsin: conservation of free energy after photoisomerization of the retinal. *J Mol Biol* 321 (4), 715-726 (2002)

47. Warshel, A. & N. Barboy: Energy storage and reaction pathway in the first step of the vision process. *Journal of the American Chemical Society* 104, 1469-1476 (1982)

48. Dioumaev, A.K., L.S. Brown, R. Needleman & J.K. Lanyi: Partitioning of free energy gain between the photoisomerized retinal and the protein in bacteriorhodopsin. *Biochemistry* 37 (28), 9889-9893 (1998)

49. Schulten, K. & P. Tavan: A mechanism for the light-driven proton pump of Halobacterium halobium. *Nature* 272 (5648), 85-86 (1978)

50. Honig, B., T. Ebrey, R.H. Callender, U. Dinur & M. Ottolenghi: Photoisomerization, energy storage, and charge separation: a model for light energy transduction in visual pigments and bacteriorhodopsin. *Proc Natl Acad Sci U S A* 76 (6), 2503-2507 (1979)

51. Kandori, H., M. Belenky & J. Herzfeld: Vibrational frequency and dipolar orientation of the protonated Schiff base in bacteriorhodopsin before and after photoisomerization. *Biochemistry* 41 (19), 6026-6031 (2002)

52. Royant, A., K. Edman, T. Ursby, E. Pebay-Peyroula, E.M. Landau & R. Neutze: Helix deformation is coupled to vectorial proton transport in the photocycle of bacteriorhodopsin. *Nature* 406 (6796), 645-648 (2000)

53. Royant, A., K. Edman, T. Ursby, E. Pebay-Peyroula, E.M. Landau & R. Neutze: Spectroscopic characterization of bacteriorhodopsin's L-intermediate in 3D crystals cooled to 170 K. *Photochem Photobiol* 74 (6), 794-804 (2001)

54. Lanyi, J.K. & H. Luecke: Bacteriorhodopsin. *Curr Opin Struct Biol* 11 (4), 415-419 (2001)

55. Hu, J.G., B.Q. Sun, A.T. Petkova, R.G. Griffin & J. Herzfeld: The predischarge chromophore in bacteriorhodopsin: a 15N solid-state NMR study of the L photointermediate. *Biochemistry* 36 (31), 9316-9322 (1997)

56. Lanyi, J.K. & B. Schobert: Mechanism of proton transport in bacteriorhodopsin from crystallographic structures of the K, L, M1, M2, and M2' intermediates of the photocycle. *J Mol Biol* 328 (2), 439-450 (2003)

57. Wampler, J.E.: Distribution analysis of the variation of B-factors of X-ray crystal structures; temperature and structural variations in lysozyme. *J Chem Inf Comput Sci* 37 (6), 1171-1180 (1997)

58. Stroud, R.M. & E.B. Fauman: Significance of structural changes in proteins: expected errors in refined protein structures. *Protein Sci* 4 (11), 2392-2404 (1995)

59. Luecke, H., H.T. Richter & J.K. Lanyi: Proton transfer pathways in bacteriorhodopsin at 2.3 angstrom resolution. *Science* 280 (5371), 1934-1937 (1998)

60. Sasaki, J., T. Yuzawa, H. Kandori, A. Maeda & H. Hamaguchi: Nanosecond time-resolved infrared spectroscopy distinguishes two K species in the bacteriorhodopsin photocycle. *Biophys J* 68 (5), 2073-2080 (1995)

61. Guex, N. & M.C. Peitsch: SWISS-MODEL and the Swiss-PdbViewer: an environment for comparative protein modeling. *Electrophoresis* 18 (15), 2714-2723 (1997)

Send correspondence to: Dr Hartmut Luecke, Department of Molecular Biology and Biochemistry, University of California, Irvine, CA 92697-3900, U.S.A., Tel: 949-824-1605, Fax: 949-824-3280, E-mail: hudel@uci.edu